PHYSICAL REVIEW B **84**, 060401(R) (2011)

Thermodynamic properties of the kagome lattice in herbertsmithite

V. R. Shaginyan,[1,2] A. Z. Msezane,[2] and K. G. Popov[3]
[1]*Petersburg Nuclear Physics Institute, Gatchina, 188300, Russia*
[2]*Clark Atlanta University, Atlanta, Georgia 30314, USA*
[3]*Komi Science Center, Ural Division, Russian Academy of Sciences (RAS), Syktyvkar, 167982, Russia*
(Received 22 May 2011; published 1 August 2011)

Strongly correlated Fermi systems are among the most intriguing and fundamental systems in physics, whose realization in some compounds is still to be discovered. We show that $ZnCu_3(OH)_6Cl_2$ can be viewed as a strongly correlated Fermi system whose low-temperature thermodynamics in magnetic fields is defined by a Fermi quantum spin liquid. Our calculations of its thermodynamic properties are in good agreement with recent experimental facts and allow us to reveal their scaling behavior which strongly resembles that observed in heavy-fermion metals and two-dimensional ^{3}He.

DOI: 10.1103/PhysRevB.84.060401 PACS number(s): 75.40.Gb, 71.27.+a, 71.10.Hf

An explanation of the rich behavior of strongly correlated Fermi systems still continues to be among the main problems in condensed-matter physics. One of the most interesting and puzzling issues in the research of strongly correlated Fermi systems is the non-Fermi-liquid (NFL) behavior detected in their thermodynamic properties. Under the application of magnetic field B, the system can be driven to a Landau Fermi-liquid behavior (LFL). Such a behavior was observed in quite different objects such as heavy-fermion (HF) metals[1,2] and two-dimensional (2D) ^{3}He.[2–4] Recently the herbertsmithite $ZnCu_3(OH)_6Cl_2$ has been exposed as a $S = 1/2$ kagome antiferromagnet[5] and experimental investigations have revealed its unusual behavior[6–9] (see Ref. 10 for a recent review). High-quality single crystals of $ZnCu_3(OH)_6Cl_2$ were synthesized and characterized,[9] the bulk properties of which are consistent with previously published powder results.[6–9] Observations have found no evidence of long-range magnetic order or spin freezing down to a temperature of 50 mK.[6–11] The specific heat C, arising from the Cu spin system, at $T < 1$ K appears to be governed by a power law with an exponent which is less than or equal to 1. At the lowest explored temperature, namely, over the temperature range $106 < T < 400$ mK, C follows a linear law temperature dependence $C \propto T$, and for temperatures of a few kelvin and higher, $C(T) \propto T^3$, and is dominated by the lattice contribution.[6–8] At low temperatures $T \leqslant 1$, the strong magnetic field dependence of the specific heat C suggests that C is predominately magnetic in origin.[6–8] It is believed that the $S = 1/2$ model on the kagome lattice can be viewed as a gapless spin liquid,[6–15] while recent accurate calculations point to a fully gapped spin liquid (see Ref. 16 and references therein). Thus, it is of crucial importance to test what kind of quantum spin liquid is formed in the herbertsmithite and determines its low-temperature thermodynamic properties. The magnetic susceptibility $\chi(T)$ of $ZnCu_3(OH)_6Cl_2$ shown in Fig. 1 displays an unusual behavior.[8] At $B \geqslant 3$ T, $\chi(T)$ has a maximum $\chi_{max}(T)$ at some temperature $T_{max}(B)$. The maximum $\chi_{max}(T)$ decreases as magnetic field B grows, while $T_{max}(B)$ shifts to higher T, reaching 15 K at $B = 14$ T. At $B \leqslant 1$ T, as seen from Fig. 1, $\chi(T) \propto T^{-\alpha}$ with $\alpha = 2/3$. The calculated exponent[2,17] is in good agreement with the experimental value $\alpha = 2/3 \simeq 0.66$.[8] The observed behavior of χ strongly resembles that in HF metals and is associated with their proximity to a quantum critical point (QCP).[2,17,18] As a result, we safely assume that a deconfined Fermi quantum spin liquid with essentially gapless excitations formed by neutral fermions is realized in $ZnCu_3(OH)_6Cl_2$ and located very near the QCP.[6] Thus, $ZnCu_3(OH)_6Cl_2$ turns out to be located at its QCP without tuning this substance to the QCP using a control parameter such as magnetic field, pressure, or chemical composition. This observation is in sharp contrast to the common practice applied to tune HF metals to their QCPs. A simple kagome lattice may have a dispersionless topologically protected branch of the spectrum with zero excitation energy that is a flat band.[19,20] In that case a fermion condensation quantum phase transition[2] (FCQPT) can be considered as the QCP of the $ZnCu_3(OH)_6Cl_2$ quantum spin liquid.

In this Rapid Communication we uncover the Fermi quantum spin liquid phase and its QCP in the herbertsmithite $ZnCu_3(OH)_6Cl_2$ and explain its low-temperature thermodynamics in magnetic fields. We calculate the susceptibility χ, magnetization M, and specific heat C as functions of temperature T versus magnetic field B. Our calculations are in good agreement with the experimental facts and allow us to reveal their scaling behavior, which strongly resembles that observed in HF metals and 2D ^{3}He.

To study the low-temperature thermodynamic and scaling behavior, we use the model of homogeneous heavy-fermion liquid.[2] This model permits to avoid complications associated with the crystalline anisotropy of solids. We propose that the quantum spin liquid is composed of fermions. These fermions with zero charge and spin $\sigma = 1/2$ occupy the corresponding Fermi sphere with the Fermi momentum p_F. The ground-state energy $E(n)$ is given by the Landau functional depending on the quasiparticle distribution function $n_\sigma(\mathbf{p})$, where $\mathbf{p}$ is the momentum. Near the FCQPT point, the effective mass M^* is governed by the Landau equation[2,21]

$$\frac{1}{M^*(T,B)} = \frac{1}{M^*} + \frac{1}{p_F^2}\sum_{\sigma_1}\int \frac{\mathbf{p}_F\mathbf{p}_1}{p_F} \times F_{\sigma,\sigma_1}(\mathbf{p_F},\mathbf{p}_1)\frac{\partial\delta n_{\sigma_1}(\mathbf{p}_1,T,B)}{\partial p_1}\frac{d\mathbf{p}_1}{(2\pi)^3}. \quad (1)$$

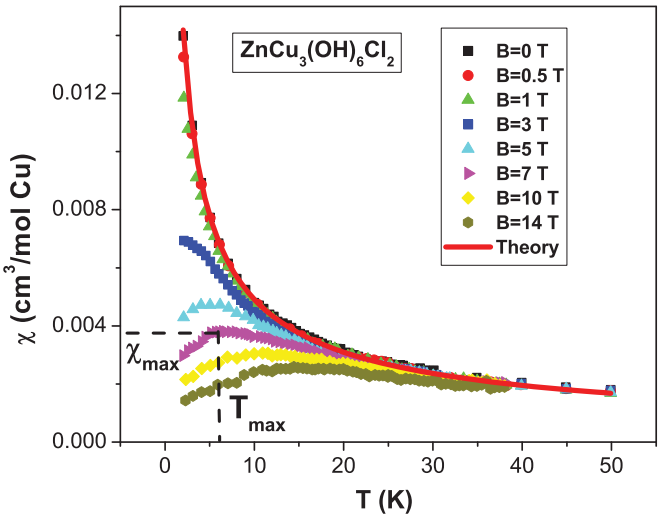

FIG. 1. (Color online) T dependence of the magnetic susceptibility χ at different magnetic fields for $ZnCu_3(OH)_6Cl_2$ (Ref. 8). The illustrative values of χ_{max} and T_{max} at $B = 7$ T are also shown. Our calculations made at $B = 0$ are depicted by the solid curve representing $\chi(T) \propto T^{-\alpha}$ with $\alpha = 2/3$.

Here we have rewritten the quasiparticle distribution function as $n_\sigma(\mathbf{p},T,B) \equiv n_\sigma(\mathbf{p},T=0,B=0) + \delta n_\sigma(\mathbf{p},T,B)$. The Landau amplitude F is completely defined by the fact that the system has to be at the QCP of the FCQPT.[2,17,22] The sole role of the Landau amplitude is to bring the system to the FCQPT point, where the Fermi surface alters its topology so that the effective mass acquires temperature and field dependence.[2,17,18] At this point, the term $1/M^*$ vanishes and Eq. (1) becomes homogeneous. It can then be solved analytically.[2,17] At $B = 0$, the effective mass strongly depends on T demonstrating the NFL behavior[2,17]

$$M^*(T) \simeq a_T T^{-2/3}. \tag{2}$$

At finite T, the application of magnetic field B drives the system to the LFL region with

$$M^*(B) \simeq a_B B^{-2/3}. \tag{3}$$

At finite B and T near the FCQPT, the solutions of Eq. (1) $M^*(B,T)$ can be well approximated by a simple universal interpolating function. The interpolation occurs between the LFL $[M^*(T) \propto \text{const}]$ and NFL $[M^*(T) \propto T^{-2/3}]$ regions.[2,17] It is convenient to introduce the normalized effective mass M_N^* and the normalized temperature T_N dividing the effective mass M^* by its maximal values M_M^* and temperature T by T_{max} at which the maximum occurs. Equation (1) allows us to calculate the thermodynamic properties for the normalized susceptibility $\chi_N = \chi/\chi_{max} = M_N^*$. Since $C/T \propto M^*$, the normalized $(C/T)_N = \chi_N = M_N^*$. We note that our calculations of M_N^* based on Eq. (1) do not contain any free fitting parameters. The normalized effective mass $M_N^* = M^*/M_M^*$ as a function of the normalized temperature $y = T_N = T/T_{max}$ is given by the interpolating function[2,17]

$$M_N^*(y) \approx c_0 \frac{1 + c_1 y^2}{1 + c_2 y^{8/3}}. \tag{4}$$

Here $c_0 = (1 + c_2)/(1 + c_1)$, where c_1 and c_2 are fitting parameters, approximating the Landau amplitude. The magnetic field B enters Eq. (1) only in the combination $\mu_B B/k_B T$, making $k_B T_{max} \simeq \mu_B B$, where k_B is the Boltzmann constant and μ_b is the Bohr magneton.[2,17] Thus, in the presence of magnetic fields the variable y becomes

$$y = T/T_{max} \simeq k_B T/\mu_B B. \tag{5}$$

The variables T and B enter Eq. (5) symmetrically; therefore Eq. (4) is valid for $y = \mu_B B/k_B T$. In what follows we use Eq. (4) to clarify our calculations based on Eq. (1). It follows directly from Eqs. (3)–(5) that $\chi(k_B T/\mu_B B)T^{2/3} \propto y^{2/3} M_N^*(y)$. Since the magnetization $M(B,T) = \int \chi(B,T)dB$, we obtain that $M(B,T)T^{-1/3}$ depends on the only variable y. These observations confirm the scaling behavior of both $\chi T^{0.66}$ and $MT^{-0.34}$, experimentally established in Ref. 8.

We are now in a position to construct the schematic phase diagram of $ZnCu_3(OH)_6Cl_2$. The phase diagram is reported in Fig. 2. At $T = 0$ and $B = 0$ the system is located at the QCP of the FCQPT without tuning. Both magnetic field B and temperature T play the role of control parameters, shifting the system from its QCP and driving it from the NFL to LFL regions, as shown by the vertical and horizontal arrows. At fixed temperatures the increase of B drives the system along the horizontal arrow from the NFL region to the LFL one. On the contrary, at fixed magnetic field and increasing temperatures the system transits along the vertical arrow from the LFL region to NFL one. The inset to Fig. 2 demonstrates the behavior of normalized effective mass M_N^* versus normalized temperature T_N following from Eq. (4). It is seen that the temperature region $T_N \sim 1$ represents a transition region between the LFL behavior with an almost constant effective mass and the NFL behavior, having $T^{-2/3}$ dependence. It is seen from Eqs. (4) and (5) and Fig. 2 that the width of the transition region $T_w \propto T \propto B$. The experimental data on measurements of χ_N,[8] $(C/T)_N = M_N^*$,[23] and our calculations

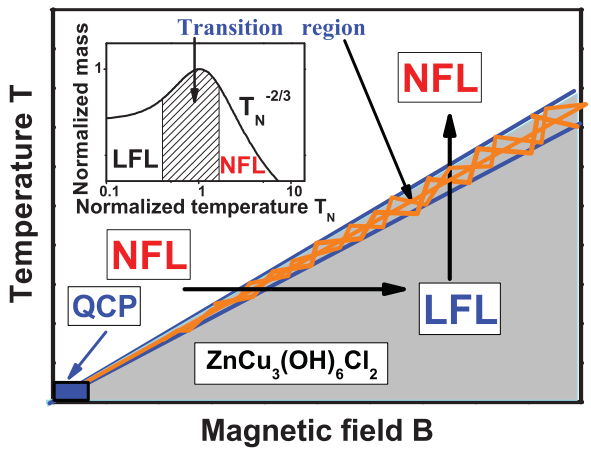

FIG. 2. (Color online) Phase diagram of $ZnCu_3(OH)_6Cl_2$. The vertical and horizontal arrows show LFL-NFL and NFL-LFL transitions at fixed B and T, respectively. The inset shows a plot of the normalized effective mass vs the normalized temperature. The transition region, where M_N^* reaches its maximum at $T_N = T/T_{max} = 1$, is shown by the arrows and the hatched area in both the main panel and in the inset.

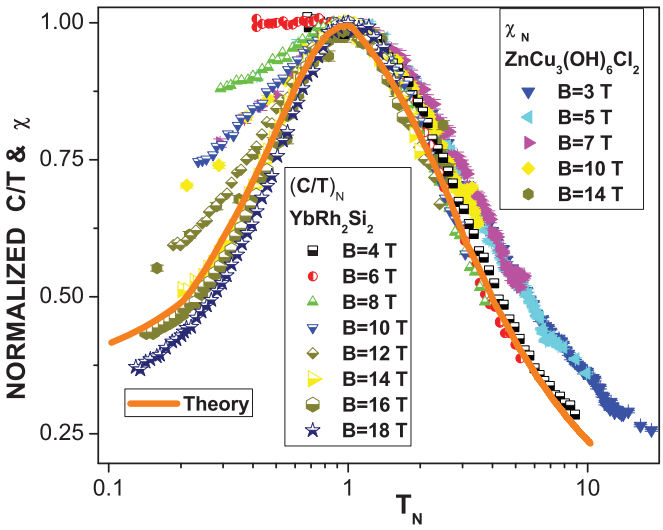

FIG. 3. (Color online) Normalized susceptibility $\chi_N = \chi/\chi_{\max} = M_N^*$ vs normalized temperature T_N. χ_N is extracted from the measurements of the magnetic susceptibility χ in magnetic fields (Ref. 8) B shown in Fig. 1. Normalized specific heat $(C/T)_N = M_N^*$ is extracted from the measurements of C/T on $YbRh_2Si_2$ in magnetic fields (Ref. 23) B. The corresponding fields B are listed in the legends. Our calculations made at field B completely polarizing the quasiparticle band are depicted by the solid curve tracing the scaling behavior of M_N^*.

of M_N^* at fixed magnetic field B that completely polarizes the quasiparticle band are shown respectively by the geometrical figures and solid curve in Fig. 3. It is clearly seen that the data collected on both $ZnCu_3(OH)_6Cl_2$ and $YbRh_2Si_2$ collapse into the same curve, obeying the scaling behavior. Consistent with the phase diagram displayed in Fig. 2, at growing temperatures ($y \simeq 1$) the LFL behavior first converts into the transition one

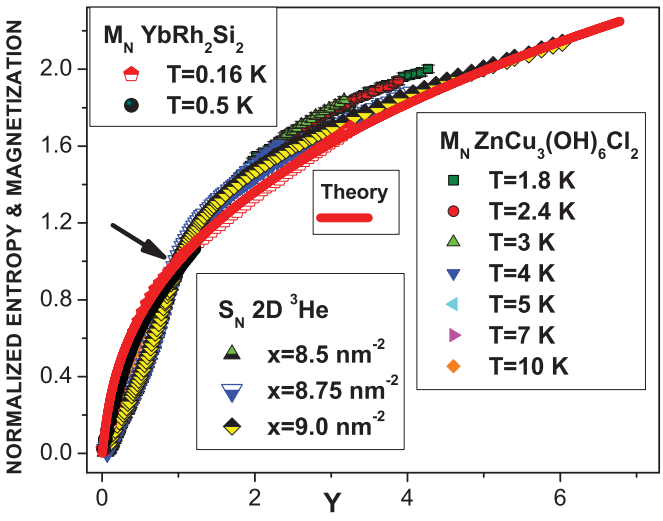

FIG. 4. (Color online) Normalized magnetization $M_N(y)$ collected on measurements of $ZnCu_3(OH)_6Cl_2$ (Ref. 8) and $YbRh_2Si_2$ (Ref. 24) at different temperatures shown in the corresponding legends. Shown by the arrow a kink is seen at $y \simeq 1$. The normalized entropy $S_N(y)$ is extracted from measurements on 2D ^{3}He (Ref. 3) at different densities x shown in the legend. The solid curve represents our calculations of the normalized magnetization.

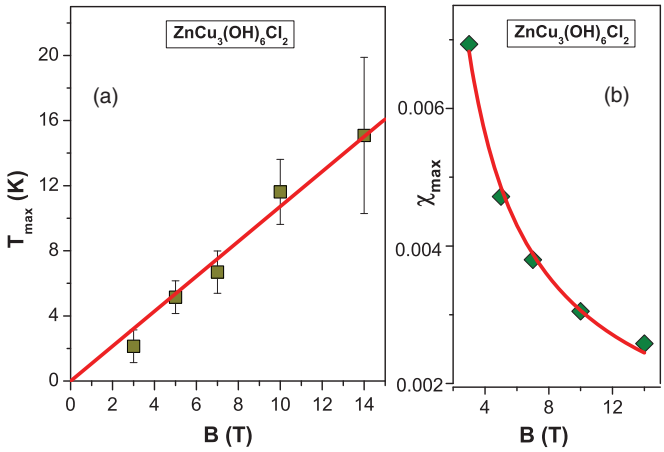

FIG. 5. (Color online) (A) The temperatures $T_{\max}(B)$ at which the maxima of χ (see Fig. 1) are located. The solid line represents the function $T_{\max} \propto aB$, and a is a parameter [see Eq. (5)]. (B) The maxima $\chi_{\max}$ of $\chi(T)$ vs magnetic field B (see Fig. 1). The solid curve is approximated by $\chi_{\max}(B) = dB^{-2/3}$ [see Eq. (3)], and d is a parameter.

and then disrupts into the NFL behavior. This demonstrates that the spin liquid of $ZnCu_3(OH)_6Cl_2$ is close to the QCP and behaves as the HF liquid of $YbRh_2Si_2$. It is seen that the low-temperature ends ($T_N \leqslant 0.5$) of the curves do not merge and their values decrease as B grows, representing the full spin polarization of the HF band at the highest reached magnetic fields.[22] Indeed, at low T_N, χ_N at $B = 14$ T is close to $(C/T)_N$ at $B = 18$ T, while our calculations shown by the solid curve are close to both functions. Both the normalized magnetization $M_N(y) = M(B/B_k)/M(B_k)$, extracted from measurements of the magnetization $M(B)$,[8] depicted by the geometrical figures, and calculated $M_N(y)$ shown by the solid line, are reported in Fig. 4. Here, T_k is the temperature at which the magnetization demonstrates the kink, while the system enters the transition region[2] shown in

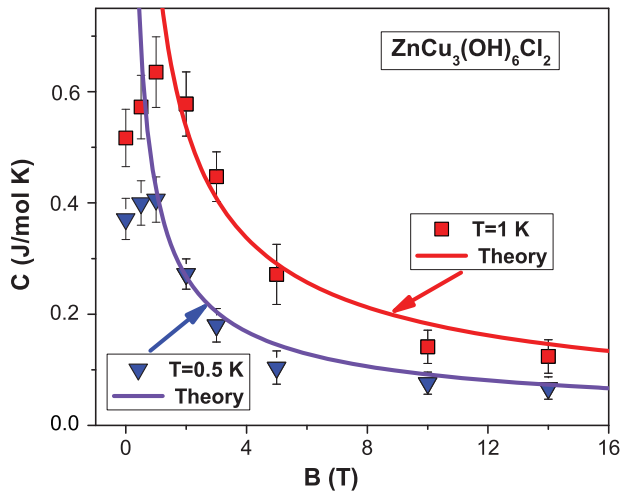

FIG. 6. (Color online) The specific heat $C(B,T)$ vs magnetic field B measured on $ZnCu_3(OH)_6Cl_2$ at two different temperatures (Ref. 6) T listed in the legends is shown by the triangles and squares. Our calculations are depicted by the solid curves, tracing the LFL behavior of $C(B,T) = a_1 B^{-2/3} T$ [see Eq. (3)], with a_1 being a parameter.

Fig. 2. The normalized entropy $S_N(y) = S(T/T_{\rm inf})/S(T_{\rm inf})$ is obtained from measurements of the entropy S on 2D ^{3}He.[3] Here $T_{\rm inf}$ is the temperature at which the system enters the transition region and S possesses its inflection point, clearly seen in the data (see the supporting online material for Ref. 3, Fig. S8, A). It is seen from Eq. (4) and from the inset to Fig. 2 that at $y < 1$, $S_N = M_N \propto y$, and at $y > 1$, $S_N = M_N \propto y^{1/3}$. This behavior produces the kink and makes the scaled data merge into a single curve in terms of the variable y. Our calculations are in good agreement with the measurements. In Fig. 5(a), the solid squares denote temperatures $T_{\rm max}(B)$ at which the maxima of $\chi(T)$ occur versus magnetic field B. In Fig. 5(b), the corresponding values of the maxima $\chi_{\rm max}(B)$ are shown by the solid diamonds versus B. It is seen that the agreement between the theory and experiment is good in the entire magnetic field domain. Our calculations of the specific heat $C(B,T)$ are shown in Fig. 6. For T of a few kelvin and higher, the lattice contribution to the specific heat is the most significant contribution. However, this contribution diminishes at low temperatures, and at $T \leqslant 1$ K, C is predominately formed by the spin liquid.[6,7] It is seen from Fig. 6 that in the LFL region at $k_B T \lesssim \mu_B B$, $C(B,T) \propto M^* T \propto B^{-2/3} T$, and field B completely defines the $M^*(B)$ behavior given by Eq. (3). Clearly, our calculations are in good agreement with the measurements when the system demonstrates LFL behavior. Indeed, at $T = 1$ K the system exhibits LFL behavior at $B \geqslant 2$ T, while at $T = 0.5$ K the LFL behavior is observed even at lower values of B, namely, $B \geqslant 1$ T.

In summary, we have shown that the kagome lattice of $ZnCu_3(OH)_6Cl_2$ can be viewed as a strongly correlated Fermi system whose thermodynamic is defined by the quantum spin liquid located at the FCQPT. Our calculations of the thermodynamic properties are in good agreement with the experimental facts, and their scaling behavior coincides with that observed in HF metals and 2D ^{3}He. We have also demonstrated that $ZnCu_3(OH)_6Cl_2$ exhibits the LFL, NFL, and the transition behavior as do HF metals and 2D ^{3}He.

We grateful to V. A. Khodel and V. A. Stephanovich for valuable discussions. This work was supported by US DOE, Division of Chemical Sciences, Office of Basic Energy Sciences, Office of Energy Research, AFOSR and the RFBR No. 09-02-00056.

[1] H. V. Löhneysen, A. Rosch, M. Vojta, and P. Wölfle, Rev. Mod. Phys. **79**, 1015 (2007).
[2] V. R. Shaginyan, M. Ya. Amusia, A. Z. Msezane, and K. G. Popov, Phys. Rep. **492**, 31 (2010).
[3] M. Neumann, J. Nyéki, and J. Saunders, Science **317**, 1356 (2007).
[4] V. R. Shaginyan, A. Z. Msezane, K. G. Popov, and V. A. Stephanovich, Phys. Rev. Lett. **100**, 096406 (2008).
[5] M. P. Shores, E. A. Nytko, B. M. Bartlett, and D. G. Nocera, J. Am. Chem. Soc. **127**, 13462 (2005).
[6] J. S. Helton, K. Matan, M. P. Shores, E. A. Nytko, B. M. Bartlett, Y. Yoshida, Y. Takano, A. Suslov, Y. Qiu, J.-H. Chung, D. G. Nocera, and Y. S. Lee, Phys. Rev. Lett. **98**, 107204 (2007).
[7] M. A. de Vries, K. V. Kamenev, W. A. Kockelmann, J. Sanchez-Benitez, and A. Harrison, Phys. Rev. Lett. **100**, 157205 (2008).
[8] J. S. Helton, K. Matan, M. P. Shores, E. A. Nytko, B. M. Bartlett, Y. Qiu, D. G. Nocera, and Y. S. Lee, Phys. Rev. Lett. **104**, 147201 (2010).
[9] T. H. Han, J. S. Helton, S. Chu, A. Prodi, D. K. Singh, C. Mazzoli, P. Müller, D. G. Nocera, and Y. S. Lee, Phys. Rev. B **83**, 100402(R) (2011).
[10] F. Bert and P. Mendels, J. Phys. Soc. Jpn. **79**, 011001 (2010).
[11] F. Mila, Phys. Rev. Lett. **81**, 2356 (1998).
[12] S. S. Lee and P. A. Lee, Phys. Rev. Lett. **95**, 036403 (2005).
[13] O. I. Motrunich, Phys. Rev. B **72**, 045105 (2005).
[14] Y. Ran, M. Hermele, P. A. Lee, and X. G. Wen, Phys. Rev. Lett. **98**, 117205 (2007).
[15] S. Ryu, O. I. Motrunich, J. Alicea, and M. P. A. Fisher, Phys. Rev. B **75**, 184406 (2007).
[16] S. Yan, D. A. Huse, and S. R. White, Science **332**, 1173 (2011).
[17] J. W. Clark, V. A. Khodel, and M. V. Zverev, Phys. Rev. B **71**, 012401 (2005).
[18] V. A. Khodel, J. W. Clark, and M. V. Zverev, Phys. Rev. B **78**, 075120 (2008).
[19] D. Green, L. Santos, and C. Chamon, Phys. Rev. B **82**, 075104 (2010).
[20] T. T. Heikkila, N. B. Kopnin, and G. E. Volovik, e-print arXiv:1012.0905v6.
[21] L. D. Landau, Sov. Phys. JETP **3**, 920 (1956).
[22] V. R. Shaginyan, K. G. Popov, V. A. Stephanovich, V. I. Fomichev, and E. V. Kirichenko, Europhys. Lett. **93**, 17008 (2011).
[23] P. Gegenwart, Y. Tokiwa, T. Westerkamp, F. Weickert, J. Custers, J. Ferstl, C. Krellner, C. Geibel, P. Kerschl, K.-H. Müller, and F. Steglich, New J. Phys. **8**, 171 (2006).
[24] P. Gegenwart, T. Westerkamp, C. Krellner, Y. Tokiwa, S. Paschen, C. Geibel, F. Steglich, E. Abrahams, and Q. Si, Science **315**, 969 (2007).